ADVANCED MATERIALS
www.advmat.de

Conductive and Elastic 3D Helical Fibers for Use in Washable and Wearable Electronics

Zihang Yang, Zirui Zhai, Zeming Song, Yingzhu Wu, Jiahao Liang, Yingfa Shan, Jinren Zheng, Haichao Liang, and Hanqing Jiang**

Due to the intrinsic properties of fabrics, fabric-based wearable systems have certain advantages over elastomeric material-based stretchable electronics. Here, a method to produce highly stretchable, conductive, washable, and solderable fibers that consist of elastic polyurethane (PU) fibers and conductive Cu fibers, which are used as interconnects for wearable electronics, is reported. The 3D helical shape results from stress relaxation of the prestretched PU fiber and the plasticity of the Cu fiber, which provides a predictable way to manipulate the morphology of the 3D fibers. The present fibers have superior mechanical and electrical properties to many other conductive fibers fabricated through different approaches. The 3D helical fibers can be readily integrated with fabrics and other functional components to build fabric-based wearable systems.

Recent advancements in materials science and micro/nanofabrication are accelerating the development of wearable electronics that can conform to the soft and curvilinear characteristics of the human body and ubiquitously monitor physiological metrics.[1] Compared with wearable electronics fabricated from elastomeric substrates (e.g., silicone-based materials),[2] fabric-based wearable systems have certain advantages due to the intrinsic attributes of the fabric, such as breathability, washability, durability, and hierarchical assembly (fiber/yarn/fabric).[3,4] To date, some academic demonstrations and commercial applications using fabric-based electronics, such as pressure sensors,[5] generators,[6] and supercapacitors,[7] have been developed. As an essential component in fabric-based wearable systems, highly conductive and preferably stretchable fibers that connect and integrate other functional components (e.g., sensors and processors) in the fabric platform[4] have been fabricated through many different approaches. The standard fabrication approach for such fibers involves the creation of core/shell structures, including coating conductive materials (e.g., metals,[8] metal nanoparticles,[9] graphite or carbon[10,11]) on fibers or embedding liquid metal in a hollow fiber shell;[12] some other methods involve the use of conductive polymers[11,13] and ionic hydrogel-based fibers.[14]

Although the abovementioned approaches are ingenious and have contributed greatly to the development of fabric-based wearable systems, some intrinsic limitations hinder the potential of these systems. The first problem is that even though some conductive fibers can be elongated to over 1000% strain,[12,14,15] the conductivity of the fiber decreases rapidly[4] upon deformation because of debonding or peeling of the conductive coating. In addition to the poor balance between stretchability and conductivity, washability—another key merit of fabric-based wearable systems—has not been appreciably addressed.[4] As an on-skin wearing device, wearable electronics require regular cleaning. However, most current conductive fibers are not washable due to the lack of insulating or protecting layers. For example, the conductive coatings (e.g., metals or graphite) on a fiber may crack or peel during washing.[4] Furthermore, another inadequately addressed issue is the ability to reliably integrate these devices with different components. Currently, conductive fibers and functional components are connected with adhesive,[12] carbon conductive tape,[16] copper tape[17] and silver paste,[17,18] which may cause safety issues. More critically, the fibers developed via the standard approach are incompatible with soldering, which is dominant on the commercial scale and is suggested as a viable way to integrate components for wearable electronics.[19] It is speculated that the metal nanoparticles or graphite coating on fibers and conductive polymers are difficult, if not impossible, to solder.

This paper presents a novel and facile method to develop a highly conductive, stretchable, 3D helical fiber made of elastic polyurethane fiber and thin copper wire that is washable and solderable, enabling integration with other functional components in a fabric platform. The fiber presented herein exhibits conductivity that is several orders of magnitude higher than other reported fibers while subjected to over 200–400% strain.

Z. Yang, Prof. Y. Wu, J. Liang, Y. Shan, J. Zheng, H. Liang
School of Textile Materials and Engineering
Wuyi University
Jiangmen, Guangdong 529020, China
E-mail: wyz@wyu.edu.cn
Z. Zhai, Prof. H. Jiang
School for Engineering of Matter
Transport and Energy
Arizona State University
Tempe, AZ 85287, USA
E-mail: hanqing.jiang@asu.edu
Dr. Z. Song
Shenzhen Xtretch Technologies Co. Ltd
Shenzhen, Guangdong 518120, China
The ORCID identification number(s) for the author(s) of this article can be found under https://doi.org/10.1002/adma.201907495.

DOI: 10.1002/adma.201907495

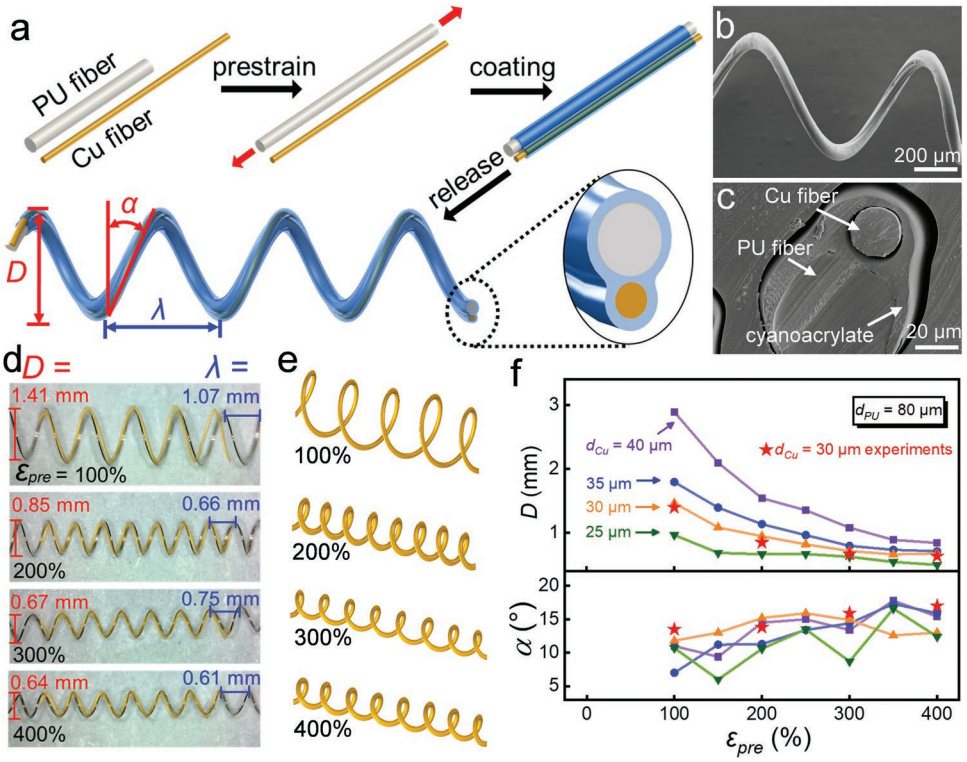

Figure 1. Fabrication and morphology 3D helical fibers. a) Fabrication process of the 3D helical fiber. b) SEM image of a 3D helical fiber with 400% prestrain. c) SEM image of the cross-sectional area of a conductive fiber with 400% prestrain. d) Optical photographs of conductive fibers with 100%, 200%, 300%, and 400% prestrains overlapped with finite element simulation results. e) 3D morphology of the finite element simulation results of conductive fibers with 100%, 200%, 300%, and 400% prestrains. f) Helix diameter D and the helical angle α from the finite element simulations for different PU fiber prestrains and Cu fiber diameters; these results are compared with experimental results with $d_{Cu} = 30$ μm.

The high conductivity and solderability is provided by the Cu wire, whereas the stretchability is provided by the 3D helical shape of the fiber. A waterproof coating on the outside of the 3D helical fiber enables washability. In this study, a power supply and LED lights are soldered to the fibers. Moreover, the excellent attributes of these fibers are demonstrated upon harsh deformation (e.g., stretching and crumpling) in water, showing unprecedented performance and characteristics for fabric-based wearable systems. These four attributes of the present fibers—stretchability, conductivity, washability, and solderability—present unique opportunities for fabric-based wearable systems.

The present method utilizes the mechanical instability of stiff thin films on soft substrates, which has been successfully implemented in early demonstrations of stretchable electronics,[20] wherein the relaxation of a prestrained soft substrate buckles the adhered stiff thin film and forms a 2D wavy structure, enabling stretchable silicon. This paper harnesses the mechanical instability in 1D fibers and describes a way to form highly stretchable 3D helical fibers. This fabrication process uses a highly stretchable polyurethane (PU) fiber (Hyosung Spandex Company) as an elastic substrate and a Cu fiber (≈95% Cu, ≈5% Sn, Longzhi Company) as a conductive material. First, the PU fiber was prestretched by a large strain ranging from 100% to 400%, firmly bonded to an intact Cu fiber via a fast-acting glue, and then wrapped with the same glue; the prestrained PU fiber was then subjected to a relaxation process to form a 3D helical shape (**Figure 1**a). PU fiber is lightweight, breathable, highly stretchable (with fracture strain up to 500%), and durable; moreover, PU fiber has been widely used in industries, from daily garments to athletic wear. The diameter of the PU fiber is ≈80 μm, whereas that of the Cu fiber ranges from 25 to 40 μm. The glue used to firmly bond the PU and Cu fibers is cyanoacrylate (M&G Stationery Company), which quickly forms a rigid thermoplastic layer between the two materials and a conformal coating on the composite fibers. Cyanoacrylate is also very stable during exposure to both moisture and household detergents. The contraction of the prestrained PU fiber buckles and twists to form a 3D helical shape. Figure S1 (Supporting Information) shows a customized tool to fabricate the 3D helical fibers. Movie S1 (Supporting Information) shows the gradual relaxation and formation of the 3D helical shape (0.25 ×, slow motion). The PU fiber in this movie has an initial length of ≈37 cm and is subjected to 300% prestrain. After relaxation, the length of the 3D helical fiber is 9 cm, which is much shorter than the undeformed length of the PU fiber because of the 3D helical shape. Figure 1b shows a scanning electron microscopy (SEM) image of a buckled helical fiber with 400% prestrain, and the cross-section of the composite fiber is shown in Figure 1c, in which the cyanoacrylate layer forms a uniform coating to provide a robust barrier for the composite fiber.

A 3D helix is described by two parameters: diameter D and helical angle α (Figure 1a). The pitch of the 3D helix λ is related

to these two parameters via $\lambda = \pi D\tan(\alpha)$. Finite element simulations were conducted to understand how the morphology of the 3D helix (i.e., D and α) depends on controllable parameters, such as prestrain ε_{pre}, the PU fiber diameter d_{PU} and the Cu fiber diameter d_{Cu}. The cyanoacrylate coating and the PU fiber were modeled as elastic materials with elastic moduli of 1.2 GPa and 42 MPa and Poisson's ratios of 0.45 and 0.32 (Figure S2, Supporting Information), respectively. The Cu fiber was characterized by an elastic-plastic material with an elastic modulus of 70 GPa, a tangent modulus of 8 GPa, and a yield stress of 400 MPa (Figure S3, Supporting Information). As detailed in the Supporting Information, Cu fibers are subjected to plastic deformation during the formation of the 3D helix as these fibers have retained the helical shape even after dissolving the PU fiber and the cyanoacrylate (Figure S4, Supporting Information). COMSOL Multiphysics was used in the simulation, for which the details are shown in the Supporting Information. The results of the simulation are compared with the results from the experiments using 80 μm diameter PU fibers and 30 μm diameter Cu fibers subjected to different prestrains. The diameter of helix D decreases from ≈1.4 to 0.6 mm as the prestrain increases from 100% to 400% (Figure 1d), which agrees very well with the simulation results overlapping in the same figure. The simulated 3D helical shapes are shown in Figure 1e.

Figure S5 (Supporting Information) illustrates that the out-of-plane bending leads to the circular shape (i.e., helix diameter D) and that the in-plane twisting is attributed to the 3D shape (i.e., pitch λ and the helical angle α). Figure 1f compares the simulation results (i.e., the lines in different colors) and the experimental results (represented by stars) for the helix diameter D and angle α for a fixed PU diameter d_{PU} = 80 μm and several Cu fiber diameters d_{Cu} = 40, 35, 30, and 25 μm. The helix diameter D decreases as the prestrain increases for the different Cu and PU fiber diameters. Under the same prestrain, thicker Cu fibers lead to larger helix diameter D. This behavior is intuitive because thicker Cu fibers have higher bending stiffness. This trend can be further shown by the strain contour and the increasing maximum strain on the Cu fiber with increasing prestrain ε_{pre} on the PU fiber (Figure S7, Supporting Information). For the same reason, the helix diameter D decreases as the PU fiber diameter d_{PU} increases (Figure S8, Supporting Information). The helical angle α is calculated using $\alpha = \arctan\left(\frac{\lambda}{\pi D}\right)$. It is interesting to note that the helical angle α exhibits a slightly increasing trend as the prestrain increases. The helical angle α is caused by the plastic deformation of the Cu fibers and characterizes the in-plane twist for the 3D helical shape. As the prestrain increases, the plastic strain in the Cu fibers increases and so does the in-plane twist, thereby leading to an increasing helical angle α. It is clear that the plasticity of the Cu fiber plays an important role in forming the 3D helical shape, as verified by a finite element simulation, in which the 3D helical shape (i.e., nonzero helical angle α) does not appear when no plasticity is considered in the model (Figure S9, Supporting Information). Experiments have shown that when different unloading paths were adopted during the release process, the helical angle α varies, due to the path-dependent behavior of plastic deformation, while the helix diameter D does not change much (Figure S10, Supporting Information). In finite element simulations, the original fiber length is much shorter than the experiments, thus the simulation cannot precisely replicate the unloading procedure in the experiments, which leads to the discrepancy in helical angle α,particularly for large prestrain (Figure 1f). Because of the decreasing trend in the helix diameter D and the increasing trend in the helical angle α in terms of increasing prestrain, the pitch $\lambda(= \pi D\tan\alpha)$ does not exhibit a clear dependence on prestrain (Figure S11, Supporting Information). Perversions were found on 3D helical fibers and are shown in Figure S12 (Supporting Information), which can be qualitatively explained by the zero twist restriction.[21] The ratio of perversion number over helical turn number is about 2.5%.

Stretchability, conductivity, washability, and solderability were tested, and the results are shown in **Figure 2**. Figure 2a shows a photograph of the relaxed and deformed helical fibers using the following parameters: ε_{pre} = 200%, d_{PU} = 80 μm, and d_{Cu} = 30 μm. In the relaxed state, the length of the helical fiber is 16 mm. The helical fiber can be deformed to ≈300% strain, at which point the Cu fiber is stretched straight and does not bear any deformation, defining a limiting deformable strain $\varepsilon_{limit} = \frac{65\text{ mm}}{16\text{ mm}} - 1$. In fact, the limiting strain can be described by the ratio of the contour length and the pitch, which is given by $\varepsilon_{limit} = \frac{\frac{\lambda}{\sin\alpha}}{\lambda} - 1 = \csc\alpha - 1$. Since the helical angle α increases with increasing prestrain (Figure 1f), the limiting strain ε_{limit} decreases as the prestrain increases, as verified in Figure 2b, which shows the stress–strain relationship of the helical fibers using different prestrains. The helical fibers are extremely soft before reaching the limiting strain ε_{limit} and become much stiffer thereafter because of the direct stretch of the Cu fibers. The equivalent stiffness before reaching the limit strain is ≈1 MPa, which is on approximately the same order of magnitude as the stiffness of the skin. The maximum stress of the composite fiber defines its strength (e.g., ≈100–150 MPa), which is on the same order of magnitude as that of the intact copper fiber (≈400 MPa). The strength of the composite fiber comes from two parts: the PU and the Cu fibers. PU fibers with larger prestrains offer greater contributions; thus, the strength of PU fibers is greater at higher prestrains. The relationship between the strength and the prestrain is detailed in the Supporting Information and shown in Figure S13 (Supporting Information). Tension fatigue tests were performed. Upon up to 10 000 loading cycles, no obvious morphological changes were observed (Figure S14, Supporting Information) and the electrical resistance keeps unchanged.

The electrical performance was tested and shown in Figure 2c, where the relative variation in the electrical resistance of the helical fiber at a fixed length (3 cm) prior to and after elongation is plotted versus the deformable strain. Neglectable variation is observed, and the maximum change is ≈0.07% at 200% deformable strain. Figure 2d compares the performance of the present work and some reported results. It is apparent that the present work outperforms all reported results in terms of both the conductivity and the relative variation in electrical resistance when the fibers are subjected to 100% deformation. Specifically, the conductivity of fibers in the present work is several orders of magnitude higher than that in many of the

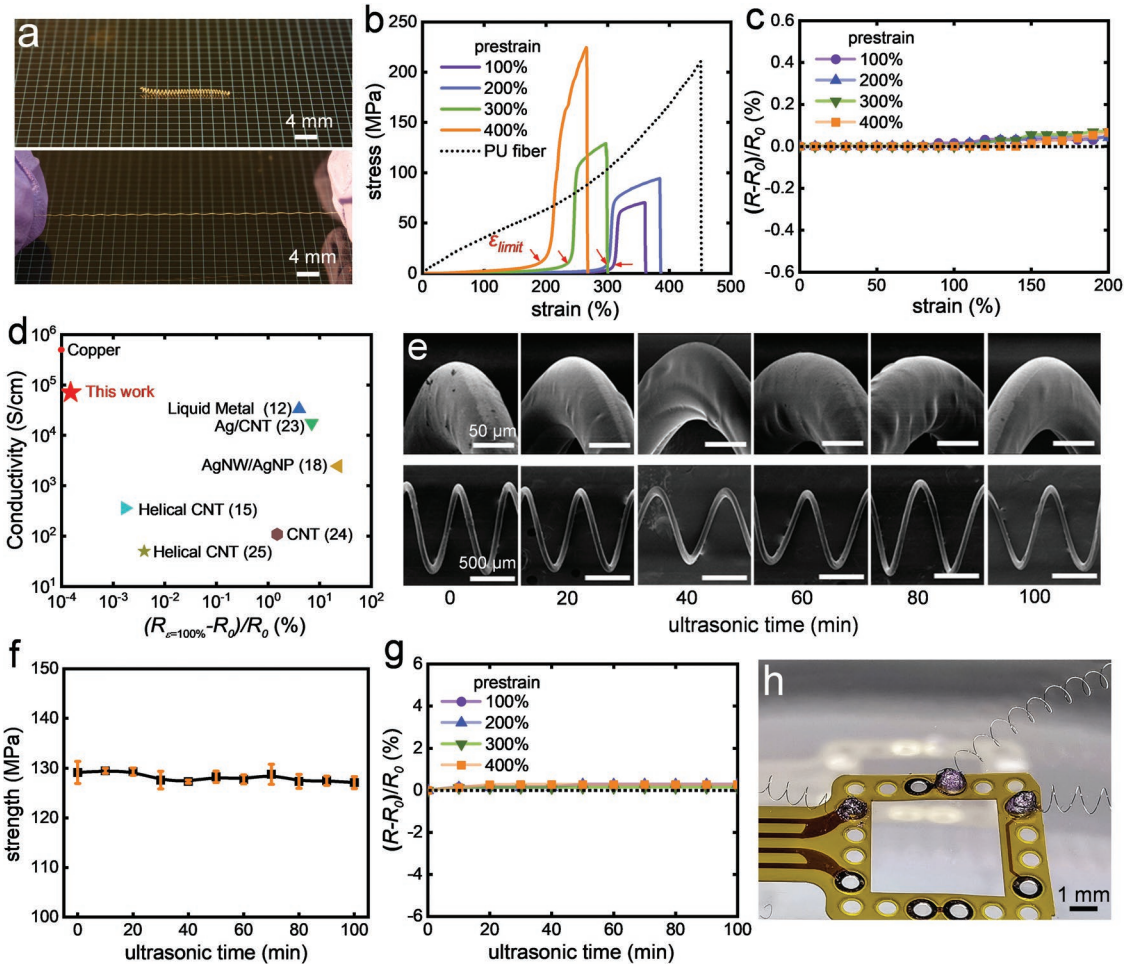

Figure 2. Mechanical, electrical, and solderable properties of 3D helical fibers. a) A 16 mm long conductive helical fiber in its relaxed state and after being stretched to 65 mm. b) Stress–strain curves of the PU fiber and the 3D helical fibers with 100%, 200%, 300%, and 400% prestrains; the limiting strains ε_{limit} are marked. c) Change in the electrical resistance of the 3D helical fibers with 100%, 200%, 300%, and 400% prestrains at different stretching strains. d) Comparison of the conductivity and electrical resistance of the present 3D helical fiber at 100% strain with those in other studies, including copper and other conductive fibers based on liquid metal,[12] silver/carbon nanotubes (Ag/CNT),[23] silver nanowires/silver nanoparticles (AgNW/AgNP),[18] carbon nanotubes (CNTs)[24] and helical CNTs.[15,25] e) SEM images (top) and magnified SEM images (bottom) of the 200% prestrained 3D helical fibers at different ultrasonic washing times from 0 to 100 min. f) Tensile strength of the 200% prestrained 3D helical fibers at different ultrasonic washing times. g) Electrical resistance of the 3D helical fibers with 100%, 200%, 300%, and 400% prestrains at different ultrasonic washing times. h) A flexible PCB soldered with three 3D helical fibers with 100% prestrain.

existing studies and is roughly on the same order of magnitude as the conductivity of the intact copper fiber. At 100% deformable strain, the fibers in the present work have the smallest resistance variation, up to five orders of magnitude smaller than other fibers (e.g., 1000% resistance change[18]). Figure S15 (Supporting Information) further shows that the electrical resistance remains nearly unchanged after 500 stretching cycles.

Ultrasonic washing, which is a much more powerful washing approach than household laundry washing, was used to remove solid particles from the object surface,[22] enabling the examination of the washability of the helical fibers. Figure 2e shows a series of SEM images of the fiber at different times under ultrasonic washing at temperature T = 20 °C. The fiber does not show obvious mechanical damage, and the morphology remains unchanged. Figure 2f presents the small variation in the mechanical strength of the 3D helical fiber at different ultrasonic washing times. Figure 2g shows the neglectable variations in the relative electrical resistance changes at different times during ultrasonic washing. Compared with other efforts to develop washable conductive fibers,[16] which produced fibers whose electrical conductivity decreases rapidly after a few minutes of ultrasonic washing, the present work is promising since washing does not induce substantial changes in the morphology, mechanical properties, or electrical resistance of the fibers produced herein. We also washed the 3D helical fibers with laundry detergent (Blue Moon, 1 mL/100 mL) and warm (35 °C)/hot water (55 °C). The same conclusion was achieved: stable mechanical and electrical performance (Figure S16, Supporting Information).

Figure 2h shows the solderability of the 3D helical fiber. Using a standard soldering process, the cyanoacrylate and PU fibers were melted at 200 °C, and the Cu fibers were exposed to form a joint with a flexible printed circuit board (PCB). A mechanical test was conducted, and the results show that the

soldered joint has strong mechanical integrity and that the fracture occurs at the fiber not at the joint (Figure S17, Supporting Information). Movie S2 (Supporting Information) further shows that the soldered piece is very robust to deformation. Since the Cu fiber is continuous, the soldering point can be formed at any location in the 3D helical fiber. After soldering two individual 3D helical fibers with electrical resistances of 15.1 and 15.8 Ω, the overall electrical resistance becomes 29.8 Ω (Figure S18, Supporting Information). The decreasing electrical resistance can be explained by the decreasing effective length of the 3D helical conductive fibers because of the soldering process. The electrical resistance at the soldering joint is calculated to be ≈0.8 Ω. Compared with other solutions to join conductive fibers (such as using silver paste), the present method is mechanically robust and electrically efficient.

Given that the diameter of the 3D helical fiber (not the helix diameter *D*) is ≈100 µm and already in the range of the diameter of the conventional cotton yarns (e.g., in the range of 200 µm), a single 3D helix can also be integrated into fabric using standard equipment. Moreover, 3D helical fibers with variable diameters from micrometers to millimeters can be made by using Cu fiber and PU fiber with different thickness, and this selection can be predicted by finite element simulations. We demonstrated that the present fibers can be woven into fabric using both knitting (**Figure 3**a) and weaving (Figure S19a, Supporting Information). SEM images (Figure 3b and Figure S19b, Supporting Information) show that the 3D helical fiber can be nicely integrated into a fabric. Particularly for knitted fabric, the thickness of the fabric is ≈1 mm, and the 3D shape of the helical fiber is nontactile. Figure 3c shows photographs of the intact and deformed knitted fabric. The force-strain relation in Figure 3d shows that the 3D helical fiber does not change the overall mechanical behavior of the knitted fabric. Compression loading test was performed and the conductivity does not change under 1.5 kg weight (Figure S20, Supporting Information). Moreover, drape testing was performed, and the results show that a silk fabric with woven 3D helical fibers does not change its drape (Figure S21, Supporting Information).

To demonstrate an integrated device with the present 3D helical fibers and other functional components, a wristband, which consists of a battery, LEDs, and the 3D helical fibers as the interconnects, was made (**Figure 4**a). The fibers perfectly fit in the textile of the wristband and cannot be distinguished. The wristband still functions when immersed in water (Figure 4b and Movie S3, Supporting Information). Figure 4c shows the functioning wristband upon 35% strain (also see Movies S4 and S5, Supporting Information). Even after exhibiting crumpling, the wristband still functions (Figure 4d and Movie S6, Supporting Information).

In summary, this paper reports a way to make highly stretchable, conductive, washable, and solderable fibers consisting of an elastic PU fiber and conductive Cu fiber; the developed fibers can be used as interconnects for wearable electronics. The formation of the 3D helical shape is a result of stress relaxation of the prestretched PU fiber and the plasticity of the Cu fiber. The morphology of the 3D fibers can be controlled by manipulating certain parameters, such as the fiber diameters and the prestrains. The present fibers have superior mechanical and electrical properties to many other conductive fibers fabricated

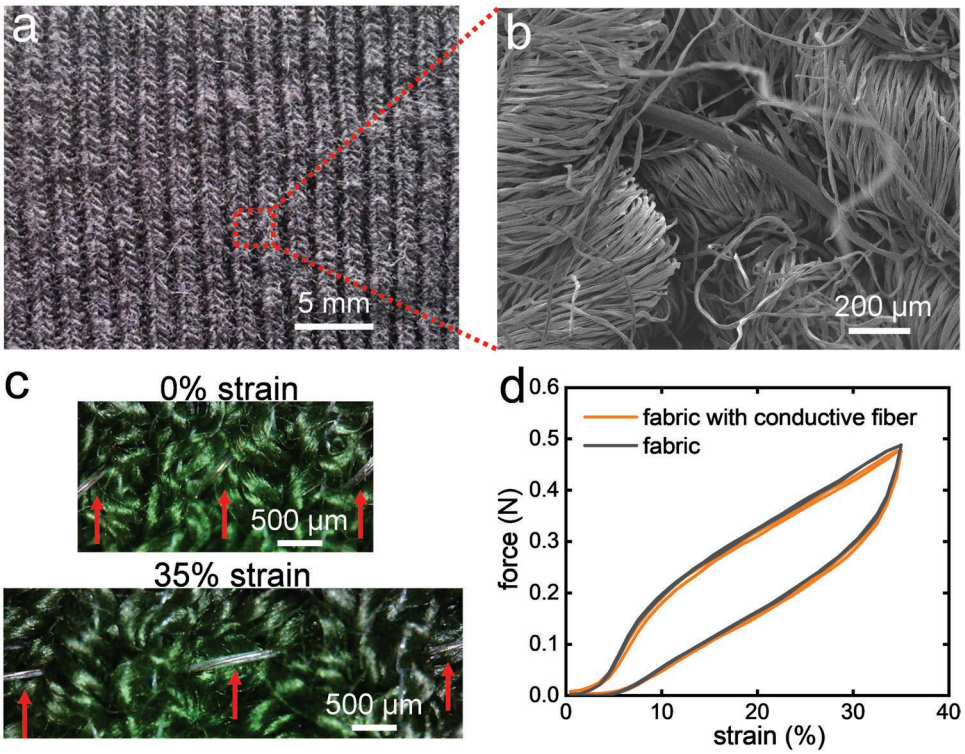

Figure 3. Performance of fabrics woven with 3D helical fibers. a) Knitted fabrics woven with 3D helical fibers. b) SEM images of the 3D helical fiber surrounded by fabric yarns. c) Knitted fabrics woven with a conductive fiber in its original state and after being stretched at 35% strain; the 3D helical fibers are marked by red arrows. d) Force-strain curves of the fabrics with or without a conductive fiber being stretched and released for 2 cycles.

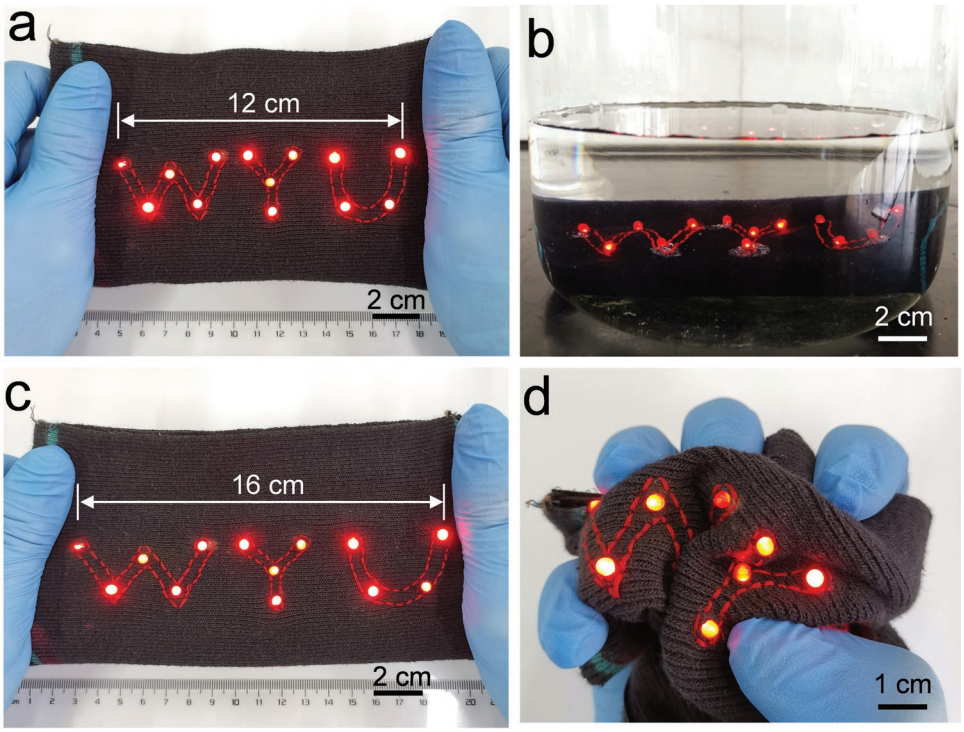

Figure 4. Performance of a wearable lighting wristband made with 3D helical fibers. a) A stretchable lighting wristband with 3D helical fibers used as interconnects; the LEDs are turned on. b) The wristband being immersed under water with the LEDs turned on. c) The wristband being stretched by hand at a 35% strain with the LEDs turned on. d) The wristband being crumpled by hand with the LEDs turned on.

through different approaches. The 3D helical fibers can be readily integrated with fabric and other functional components to build fabric-based wearable systems. The strategy of producing 3D helical fibers can be used to design devices with other functions, such as stretchable heaters, circuits and optical fibers.

Supporting Information

Supporting Information is available from the Wiley Online Library or from the author.

Acknowledgements

Z.Y. and Z.Z. contributed equally to this work. Y.W. acknowledges financial support from the Guangdong Province Special Innovation Project (2017KTSCX182). H.J. acknowledges support from the guest professorship of Wuyi University and the Global Sports Initiative at Arizona State University.

Conflict of Interest

The authors declare no conflict of interest.

Keywords

3D helical shape, conductive fibers, stretchable and washable electronics, wearable electronics

Received: November 14, 2019
Revised: December 17, 2019
Published online:

[1] D.-H. Kim, N. Lu, R. Ma, Y.-S. Kim, R.-H. Kim, S. Wang, J. Wu, S. M. Won, H. Tao, A. Islam, K. J. Yu, T.-i. Kim, R. Chowdhury, M. Ying, L. Xu, M. Li, H.-J. Chung, H. Keum, M. McCormick, P. Liu, Y.-W. Zhang, F. G. Omenetto, Y. Huang, T. Coleman, J. A. Rogers, *Science* **2011**, *333*, 838.
[2] J. A. Rogers, T. Someya, Y. Huang, *Science* **2010**, *327*, 1603.
[3] M. Stoppa, A. Chiolerio, *Sensors* **2014**, *14*, 11957.
[4] W. Zeng, L. Shu, Q. Li, S. Chen, F. Wang, X. M. Tao, *Adv. Mater.* **2014**, *26*, 5310.
[5] J. Lee, H. Kwon, J. Seo, S. Shin, J. H. Koo, C. Pang, S. Son, J. H. Kim, Y. H. Jang, D. E. Kim, *Adv. Mater.* **2015**, *27*, 2433.
[6] J. Zhong, Y. Zhang, Q. Zhong, Q. Hu, B. Hu, Z. L. Wang, J. Zhou, *ACS Nano* **2014**, *8*, 6273.
[7] K. Jost, D. Stenger, C. R. Perez, J. K. McDonough, K. Lian, Y. Gogotsi, G. Dion, *Energy Environ. Sci.* **2013**, *6*, 2698.
[8] a) X. Jin, C. Xiao, S. An, G. Jia, *J. Mater. Sci.* **2007**, *42*, 4384; b) N. J. Pinto, P. Carrión, J. X. Quiñones, *Mater. Sci. Eng., A* **2004**, *366*, 1; c) D. Zabetakis, M. Dinderman, P. Schoen, *Adv. Mater.* **2005**, *17*, 734.
[9] G. Mattana, P. Cosseddu, B. Fraboni, G. G. Malliaras, J. P. Hinestroza, A. Bonfiglio, *Org. Electron.* **2011**, *12*, 2033.
[10] a) G. Che, B. Lakshmi, C. Martin, E. Fisher, R. S. Ruoff, *Chem. Mater.* **1998**, *10*, 260; b) Z. Li, G. Luo, F. Wei, Y. Huang, *Compos. Sci. Technol.* **2006**, *66*, 1022; c) W. Thongruang, R. J. Spontak, C. M. Balik, *Polymer* **2002**, *43*, 3717.
[11] A. Soroudi, M. Skrifvars, *Synth. Met.* **2010**, *160*, 1143.
[12] S. Zhu, J.-H. So, R. Mays, S. Desai, W. R. Barnes, B. Pourdeyhimi, M. D. Dickey, *Adv. Funct. Mater.* **2013**, *23*, 2308.
[13] a) B. Kim, V. Koncar, E. Devaux, C. Dufour, P. Viallier, *Synth. Met.* **2004**, *146*, 167; b) C. R. Ríos-Soberanis, R. A. Ley-Bonilla, R. H. Cruz-Estrada, C. V. Cupul-Manzano, L. M. Rangel-Rodríguez, A. Caballero-Can, *Polym. Int.* **2009**, *58*, 817; c) A. J. Granero, P. Wagner, K. Wagner, J. M. Razal, G. G. Wallace, M. in het Panhuis,

Adv. Funct. Mater. **2011**, *21*, 955; d) P. Sukitpaneenit, T. Thanpitcha, A. Sirivat, C. Weder, R. Rujiravanit, *J. Appl. Polym. Sci.* **2007**, *106*, 4038.
[14] T. Yin, L. Wu, T. Wu, G. Mao, G. Nian, Z. Chen, X. Hu, P. Wang, Y. Xiang, H. Yu, *J. Polym. Sci., Part B: Polym. Phys.* **2019**, *57*, 272.
[15] Z. Liu, S. Fang, F. A. Moura, J. Ding, N. Jiang, J. Di, M. Zhang, X. Lepró, D. Galvao, C. Haines, *Science* **2015**, *349*, 400.
[16] Y. Wei, S. Chen, X. Yuan, P. Wang, L. Liu, *Adv. Funct. Mater.* **2016**, *26*, 5078.
[17] Y. Cheng, R. Wang, J. Sun, L. Gao, *Adv. Mater.* **2015**, *27*, 7365.
[18] S. Lee, S. Shin, S. Lee, J. Seo, J. Lee, S. Son, H. J. Cho, H. Algadi, S. Al-Sayari, D. E. Kim, *Adv. Funct. Mater.* **2015**, *25*, 3114.
[19] G. S. Jeong, D.-H. Baek, H. C. Jung, J. H. Song, J. H. Moon, S. W. Hong, I. Y. Kim, S.-H. Lee, *Nat. Commun.* **2012**, *3*, 977.
[20] D. Y. Khang, H. Q. Jiang, Y. Huang, J. A. Rogers, *Science* **2006**, *311*, 208.
[21] a) J. Huang, J. Liu, B. Kroll, K. Bertoldi, D. R. Clarke, *Soft Matter* **2012**, *8*, 6291; b) J. Liu, J. Huang, T. Su, K. Bertoldi, D. R. Clarke, *PLoS One* **2014**, *9*, e93183; c) S. Liu, Z. Yao, K. Chiou, S. I. Stupp, M. O. De La Cruz, *Proc. Natl. Acad. Sci. USA* **2016**, *113*, 7100.
[22] W. Kim, T.-H. Kim, J. Choi, H.-Y. Kim, *Appl. Phys. Lett.* **2009**, *94*, 081908.
[23] R. Ma, B. Kang, S. Cho, M. Choi, S. Baik, *ACS Nano* **2015**, *9*, 10876.
[24] S. Jiang, H. Zhang, S. Song, Y. Ma, J. Li, G. H. Lee, Q. Han, J. Liu, *ACS Nano* **2015**, *9*, 10252.
[25] W. Son, S. Chun, J. M. Lee, Y. Lee, J. Park, D. Suh, D. W. Lee, H. Jung, Y.-J. Kim, Y. Kim, *Nat. Commun.* **2019**, *10*, 426.